Front. Phys., 2012, 7(6): 637–646
DOI 10.1007/s11467-012-0273-9

REVIEW ARTICLE

A brief review of antimatter production

Yu-Gang Ma[1,†], **Jin-Hui Chen**[1], **Liang Xue**[1,2]

[1] *Shanghai Institute of Applied Physics, Chinese Academy of Sciences, Shanghai 201800, China*
[2] *University of Chinese Academy of Sciences, Beijing 100080, China*
E-mail: †*ygma@sinap.ac.cn*

Received August 29, 2012; accepted October 10, 2012

In this article, we present a brief review of the discoveries of kinds of antimatter particles, including positron ($\overline{\mathrm{e}}$), antiproton ($\overline{\mathrm{p}}$), antideuteron ($\overline{\mathrm{d}}$) and antihelium-3 ($^{3}\overline{\mathrm{He}}$). Special emphasis is put on the discovery of the antihypertriton(${}^{3}_{\overline{\Lambda}}\overline{\mathrm{H}}$) and antihelium-4 nucleus ($^{4}\overline{\mathrm{He}}$, or $\overline{\alpha}$) which were reported by the RHIC-STAR experiment very recently. In addition, brief discussions about the effort to search for antinuclei in cosmic rays and study of the longtime confinement of the simplest antimatter atom, antihydrogen are also given. Moreover, the production mechanism of anti-light nuclei is introduced.

Keywords antimatter, $\overline{\mathrm{e}}$, $\overline{\mathrm{p}}$, $\overline{\mathrm{d}}$, $^{3}\overline{\mathrm{H}}$, ${}^{3}_{\overline{\Lambda}}\overline{\mathrm{H}}$, $^{3}\overline{\mathrm{He}}$, $^{4}\overline{\mathrm{He}}$

PACS numbers 25.75.Dw, 13.85.Ni

Contents

1 Introduction

The ideal of antimatter can be traced back to the end of 1890s, when Schuster discussed the possibility of the existence of antiatoms as well as antimatter solar system by hypothesis in his letter to Nature magazine [1]. However, the modern concept of antimatter is originated from the negative energy state solution of a quantum-mechanical equation, which was proposed by Dirac in 1928 [2]. Two years later, Chao found that the absorption coefficient of hard γ-rays in heavy elements was much larger than that to be expected from the Klein–Nishima formula or any other [3, 4]. This “abnormal” absorption is in fact due to the production of the pair of electron and its anti-partner, so-called positron. Therefore Chao’s experiment is the first indirect observation of the first anti-matter particle, namely positron, in the history. Another two years later, Anderson observed positron with a cloud chamber [5]. Antimatter nuclei such as $\overline{\mathrm{d}}$, $^{3}\overline{\mathrm{H}}$, $^{3}\overline{\mathrm{He}}$ have been widely studied in both cosmic rays [6–8] and accelerator experiments [9–15] for the purposes of dark matter exploration and the study of manmade matter such as quark gluon plasma (QGP) respectively, since the observation of anti-proton ($\overline{\mathrm{p}}$) [16] in 1955. The possibility of the anti-gravity behavior between matter and antimatter has been discussed somewhere else [17]. The recent progress regarding the observation of antihypertriton (${}^{3}_{\overline{\Lambda}}\overline{\mathrm{H}}$) [18] and antihelium-4 ($^{4}\overline{\mathrm{He}}$, or $\overline{\alpha}$) [19] nucleus in high energy heavy ion collisions [20–22] reported by RHIC-STAR experiment as well as the longtime confinement of antihydrogen atoms [23] based on an antiproton decelerator facility by CERN (the European Organization for Nuclear Research) ALPHA collaboration have already created a lot of excitation in both of the nuclear and particle physics community. All of the measurements performed above have implications beyond the fields of their own. For example, the study of hypernucleus in heavy ion collisions is essential for the understanding of the interaction between nucleon and hyperon (YN interaction), which plays an important role in the explanation of the structure of neutron star. Furthermore, as we learned from heavy ion collisions, the production rate for $^{4}\overline{\mathrm{He}}$ produced by colliding the high energy cosmic rays with interstellar materials is too low to be observed. Even one $^{4}\overline{\mathrm{He}}$ or heavier antinucleus observed in the cosmic rays should be a great hint of the existence of massive antimatter in the Universe. Finally, the successful trap of antihydrogen atoms leads to a precise test of the CPT symmetry law, as well as a measurement of the gravitational effects between antimatter and matter in the future.

In this article, we present a review of kinds of antimatter particles experimentally, based on the time schedule of their first time observations. The paper is arranged as follows: In Section 2, we will take a look back to the discoveries of positron and antiproton. In Section 3, the first time observations of antideuteron and antihelium-3 will be discussed. Section 4 presents a brief review of the formation and observation of ${}^{3}_{\Lambda}\overline{\mathrm{H}}$ through their secondary vertex reconstructions via decay channel ${}^{3}_{\Lambda}\overline{\mathrm{H}} \rightarrow {}^{3}\overline{\mathrm{He}} + \pi^{+}$ with a branch ratio of 25% in high energy heavy ion collisions. In Section 5, we have discussion of the particle identification of ${}^{4}\overline{\mathrm{He}}$ nucleus by measuring their mass value directly with the fully installed detector Time Of Flight (TOF) at RHIC-STAR. In Section 6, we discuss the effort of searching for antinuclei in cosmos. In Section 7, the longtime trap of antihydrogen atoms performed by ALPHA experiment is introduced. In the last section, we have a discussion on antimatter nuclei production mechanism. Finally we give a summary and outlook.

2 Observation of positron

In 1930, Chao performed a few γ-ray scattering experiments on different elements [3, 4]. γ-rays from Th C after being filtered through 2.7cm of Pb were used as the primary beam. Al and Pb were chosen as the represensitives of the light and the heavy elements. For Al the γ-scattering is, within experimental error, that predicted by the Klien–Nishima formula which assumes that the removal of the energy from the primary beam is entirely due to Compton scattering of the extranuclear electrons. However, for Pb additional scattering rays were observed. The wavelength and space distribution of these rays are inconsistent with an extranuclear scatterer [3, 4]. Later on, this abnormal absorption was identified as the outcome of the process of electron-positron pair production. Therefore this experiment was also the first experimental indiction of the first anti-matter particle, positron, in the observation history for the antimatter.

Two years later, Anderson identified 15 positive tracks by photographing the cosmic rays with a vertical Wilson chamber in August, 1932 [5]. The unknown particles were recognized as the predicted antimatter electron (positron) after an analysis of their energy loss, ionization, as well as their curvatures in the chamber. Figure 1 shows that, a positron reduces its energy by passing through a 6 mm lead plate in the cloud chamber. The track length from the upper part of the cloud chamber can only be interpreted with the observation of positron.

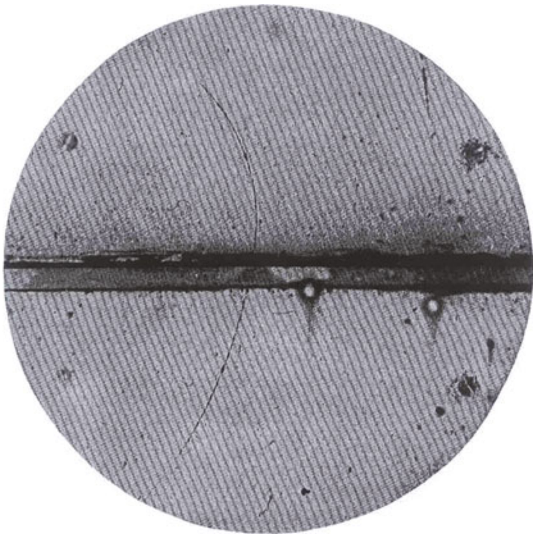

Fig. 1 A photograph for the discovery of positron from Ref. [5]. The curvature stands for a comic ray passing through a 6 mm lead plate with a reduction of its energy. The length of the latter part can only be interpreted with the appearance of antimatter electron.

3 Observations of antiproton, antideuteron and antihelium-3

Physicists had expanded their understanding of the natural world, and took into consideration that every particle should have their antimatter partner after the discovery of positron. They were able to expand their knowledge of antimatter with the development of the technology of accelerators, while the development of Time-of-Flight detector system played an important role in the following identification of antimatter particles. In the year 1955, Chamberlain and Segrè from University of California reported their observation of antiprotons based on the Bevatron facility [16]. Antiprotons were produced and scattered into the forward direction by projecting a bunch of proton beam to the copper target at Bevatron. By observing the times of flight for antiprotons, this experiment made more sense by the fact that the electronic gate time is considerably longer than the spread of observed antiproton flight times. The electronic equipment accepts events that are within ±6 millimicroseconds of the right flight time for antiprotons, while the actual antiproton traces recorded show a grouping of fight times to ±1 or 2 millimicroseconds. Figure 2(a) and (b) depict a histogram of meson flight times and that of antiproton flight times, respectively. Accidental coincidences account for many of the sweeps (about 2/3 of the sweeps) during the runs designed to detect antiprotons. A histogram of the apparent flight times of accidental coincidences is shown in Fig. 2(c). It will be noticed that the accidental coincidences do not show the close grouping of flight times characteristic of the antiproton or meson

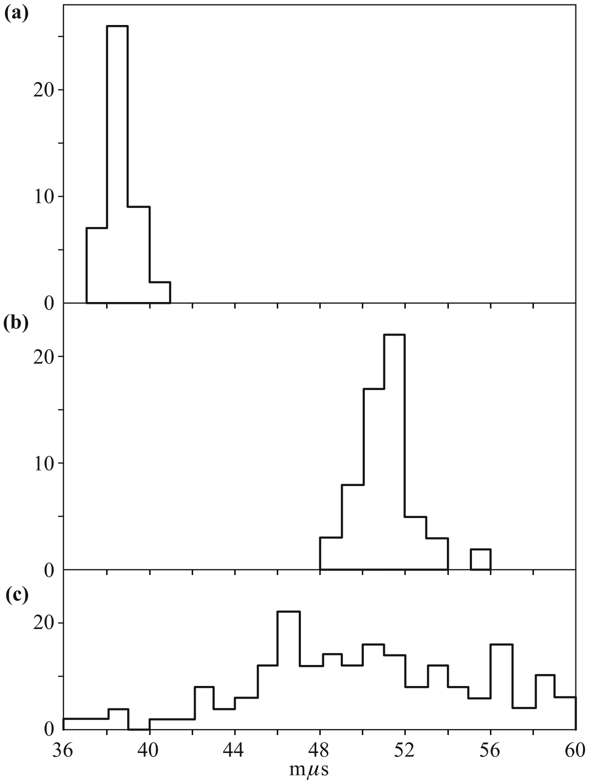

Fig. 2 **(a)** Histogram of meson times used for calibration. **(b)** Histogram of antiproton flight times. **(c)** Apparent flight times of a representative accidental coincidences. Times of flight are in units of 10^{-9} s. The ordinates show the number of events in each 10^{-10} second intervals. Reproduced from Ref. [16], Copyright © 1955 American Physical Society.

flight times. In total, 60 antiprotons were detected, with their mass measured and found to be equal to protons within uncertainties based on the detectors at Bevatron [16].

Antideuteron was observed by Alternating Gradient Synchrotron (AGS) [9] at BNL and later confirmed by Proton Synchrotron (PS) [24] at CERN in 1965. Both of the experiments were implemented by colliding protons with beryllium. The data was collected with a set of time of flight system S_1S_{10} (210 ft) and S_2S_9 (170 ft) at AGS. Figure 3 shows the travel time of antideuterons between detectors S_2 and S_9 at different momentum region. The time to channel calibration is 0.56 ns per channel. The peak positions from Fig. 3 moves from channel 21.5 at $p = 6$ GeV/c to channel 23.5 at 5.4 GeV/c, and to channel 26 at 5.0 GeV/c, corresponding to $\Delta\beta/\Delta p = (1.6\pm0.4)\times10^{-2}(\mathrm{MeV/c})^{-1}$. The calculated mass equals to 1.86 GeV/c via formula $\mathrm{d}\beta/\mathrm{d}p = \beta^3 m^2/p^3$, and is interpreted to be antideuteron.

Experiments with antimatter nuclei heavier than antideuteron were implemented at the Institute of High Energy Physics, Russia. Five antihelium-3 [10, 11] were produced by colliding the 70 GeV proton beams with aluminum target. The calculated charge is $(0.99 \pm 0.03)2e$, while the measured mass equals to $(1.00\pm0.03)3m_p$. The differential production cross section of antihelium-3 with momentum to 20 equal GeV/c at $\theta = 27$ mrad was calculated and found to be 2.0×10^{-35} $\mathrm{cm}^2/\mathrm{sr}\cdot\mathrm{GeV/c}$ per aluminum nucleus. While the differential cross section for π^- is 1.5×10^{-25} $\mathrm{cm}^2/\mathrm{sr}\cdot\mathrm{GeV/c}$ per aluminum nucleus. The ratio between differential cross section of antihelium-3 and pion is 1.3×10^{-10}. Figure 4 shows an atomic number dependence of the ratios. The ratios decrease by a magnitude of four orders with each additional nucleon added. By extrapolating the distribution to larger mass area, the relative cross section of antihelium-4 is about 10^{-14}.

4 Observation of ${}^{3}_{\bar{\Lambda}}\overline{\mathrm{H}}$

Unlike the normal nuclei, (anti-) nuclei, (anti-)

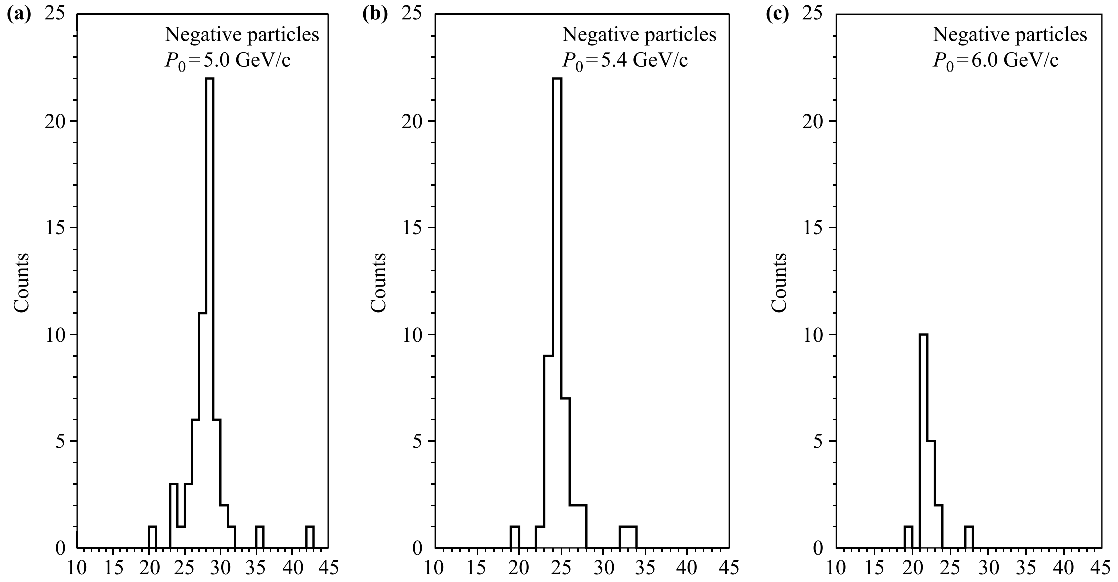

Fig. 3 The evidence for the observation of antideuteron from Ref. [9]. **(a)**, **(b)** and **(c)** shows the time-of-flight distribution for particles between counters S_2 and S_9 with 0.56 ns per channel. Reproduced from Ref. [9], Copyright © 1965 American Physical Society.

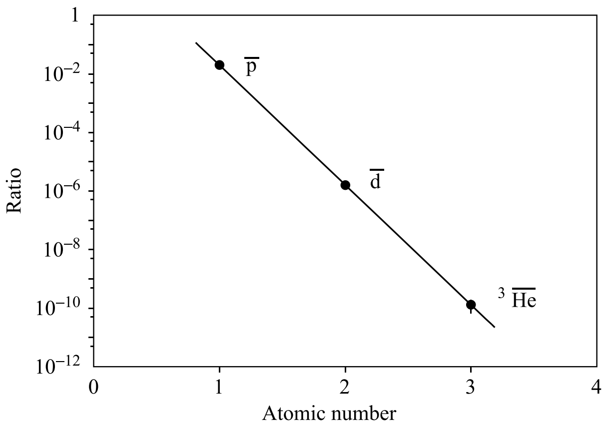

Fig. 4 Atomic number dependence of the relative production of antimatter nuclei with respect to pion with fixed momentum at 20 GeV/c and θ equal to 27 mrad. Reproduced from Refs. [10, 11], Copyright © 1970 Springer and Copyright © 1971 Elsevier, respectively.

hypernucleus includes the (anti-) strange quark degree of freedom, of which the typical one is Λ-hypernucleus. The simplest hypernucleus observed so far is hypertriton, which is composed of one neutron, one proton and one Λ-hyperon. Hypernucleus provides an ideal environment to study the hyperon–nucleon (YN) interaction, responsible in part for the binding of hypernuclei, which is of fundamental interest in nuclear physics and nuclear astrophysics. In previous research history, quite a lot of hypernuclei have been discovered, even for the observation of double-Λ hypernucleus [25], but still no anti-hypernucleus was observed until the STAR collaboration announced the first anti-matter hypernucleus, i.e. $^{3}_{\Lambda}\overline{\mathrm{H}}$ [18], in 2010. The observation of $^{3}_{\Lambda}\overline{\mathrm{H}}$ can be achieved by reconstructing their secondary vertex via $^{3}_{\Lambda}\overline{\mathrm{H}} \rightarrow {}^{3}\overline{\mathrm{He}} + \pi^{+}$ [18, 20]. The data used for analysis was collected by STAR experiment at Relativistic Heavy Ion Collider (RHIC), by use of the cylindrical Time Projection Chamber (TPC), which is 4 meters in the diameter direction and 4.2 meters long in the beamline direction [26]. TPC is able to reconstruct charged tracks between ±1.8 units of pseudo-rapidity with full azimuthal angle. The identification of tracks can be achieved by correlating their ionization energy loss $\langle \mathrm{d}E/\mathrm{d}x \rangle$ in TPC with their magnetic rigidity. Figure 4(c) shows $\langle \mathrm{d}E/\mathrm{d}x \rangle$ for negative tracks versus the magnetic rigidity. The different bands stand for different kinds of particles. Figure 5 is the distribution of a new variable, $z = Ln(\langle \mathrm{d}E/\mathrm{d}x \rangle / \langle \mathrm{d}E/\mathrm{d}x \rangle_B)$,which is used to identify $^{3}\mathrm{He}$ and $^{3}\overline{\mathrm{He}}$, where $\langle \mathrm{d}E/\mathrm{d}x \rangle_B$ is the expected value of $\langle \mathrm{d}E/\mathrm{d}x \rangle$. Approximately, a sample of 5810 $^{3}\mathrm{He}$ and 2168 $^{3}\overline{\mathrm{He}}$ were collected for the secondary vertex reconstruction of $^{3}_{\Lambda}\overline{\mathrm{H}}$.

Topological cuts including the distance between two daughter tracks $^{3}\overline{\mathrm{He}}$ and π^{+} (<1 cm), distance of closest approach (DCA) between $^{3}_{\Lambda}\overline{\mathrm{H}}$ and primary vertex (<1 cm), decay length of $^{3}_{\Lambda}\overline{\mathrm{H}}$ (>2.4 cm), and the DCA of π track (>0.8 cm), are employed to promote the signal to background ratio. The invariant mass of $^{3}_{\Lambda}\mathrm{H}$ and $^{3}_{\Lambda}\overline{\mathrm{H}}$ were calculated based on the conservation of momentum and energy in the decay process. The results are shown in Fig. 5(a) for $^{3}_{\Lambda}\mathrm{H}$ and Fig. 4(b) for $^{3}_{\Lambda}\overline{\mathrm{H}}$. The successfully reproduced combinatorial background with a rotation

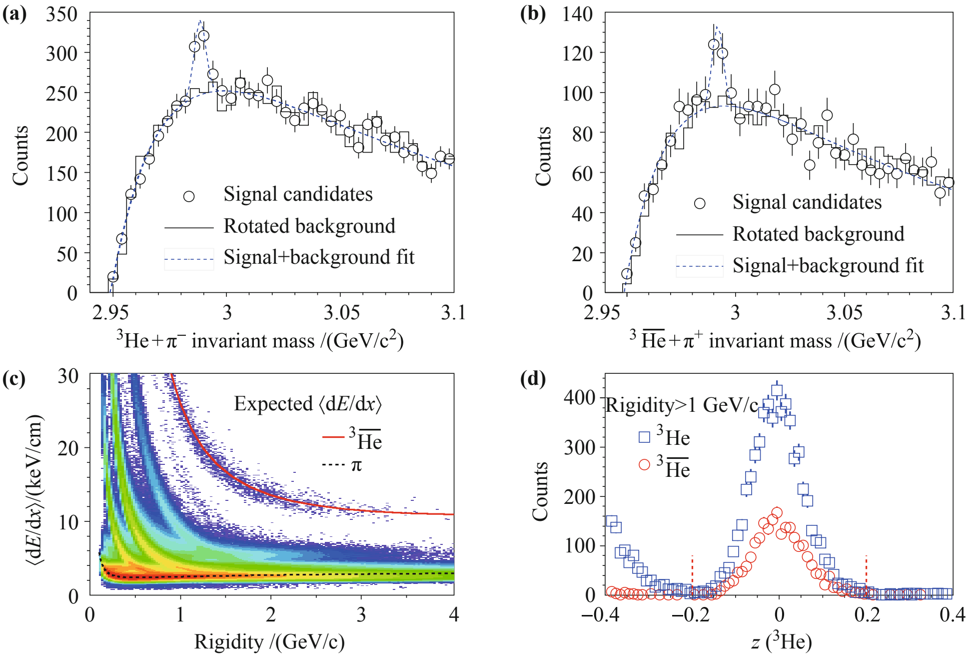

Fig. 5 **(a)**, **(b)** Reconstructed invariant mass distribution of $^{3}\mathrm{He}$ and π, open circles stand for the signal distribution, while solid lines are the rotated combination background. Blue dashed lines are the Gaussian (signal) plus double exponential (background) function fit to the distribution. **(c)** $\langle \mathrm{d}E/\mathrm{d}x \rangle$ as a function of rigidity ($p/|Z|$) for negative particles, and theoretical $\langle \mathrm{d}E/\mathrm{d}x \rangle$ value for $^{3}\overline{\mathrm{He}}$ and π are also plotted. **(d)** shows that a clean $^{3}\mathrm{He}$ and $^{3}\overline{\mathrm{He}}$ sample can be obtained with cut $|z(^{3}\mathrm{He})| < 0.2$. Reproduced from Ref. [18], Copyright © 2010 American Association for the Advancement of Science.

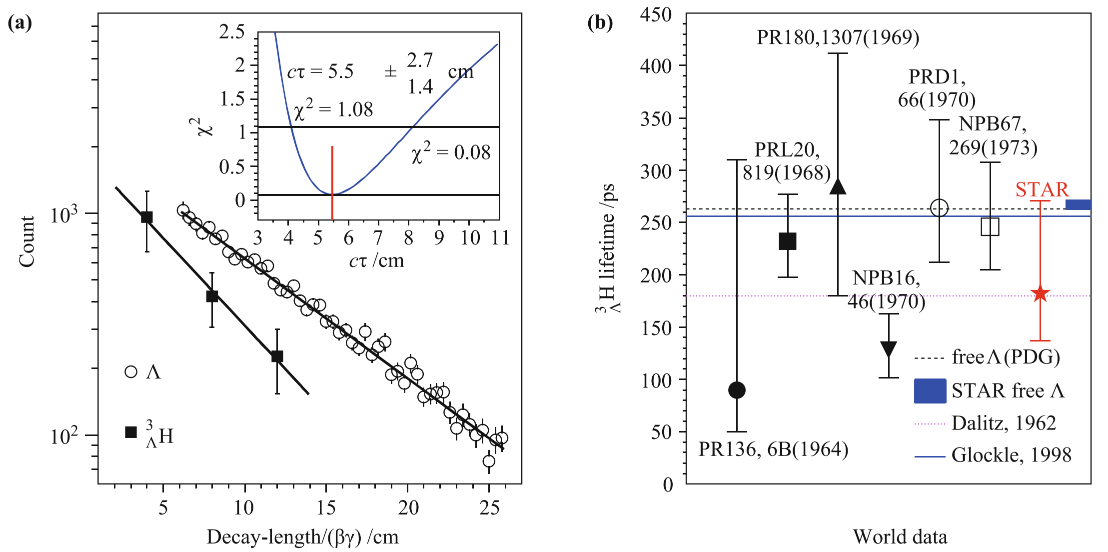

Fig. 6 (a) The yields of $^3_\Lambda\overline{\mathrm{H}}$ (*solid squares*) and Λ (*open circles*) vs $c\tau$ distribution. The solid lines stand for the $c\tau$ fits, and the insert plot describes χ^2 distribution of the best fits. (b) Comparison between the present measurement and theoretical calculation [27, 28], as well as the previous measurements [29–34]. Reproduced from Ref. [18], Copyright © 2010 American Association for the Advancement of Science.

strategy can be described by double exponential function: $f(x) \propto \exp[-(x/p_1)] - \exp[-(x/p_2)]$, where $x = m - m(^3\mathrm{He}) - m(\pi)$, and p_1, p_2 are the parameters. Finally, the signals are counted by subtracting the double exponential background of $^3_\Lambda$H and $^3_\Lambda\overline{\mathrm{H}}$. In total, 157 ± 30 of $^3_\Lambda$H and 70 ± 17 of $^3_\Lambda\overline{\mathrm{H}}$ are observed.

The measurement of $^3_\Lambda$H ($^3_\Lambda\overline{\mathrm{H}}$) lifetime provides us an effective tool to understand the Y(Λ)–N(p,n) interactions [27, 28]. And, the secondary vertex reconstruction of $^3_\Lambda$H ($^3_\Lambda\overline{\mathrm{H}}$) makes us to be able to perform a calculation of its lifetime, via equation $N(t) = N(0)\exp(-t/\tau)$, where $t = l/(\beta\gamma c)$, $\beta\gamma c = p/m$, l is the decay length of $^3_\Lambda$H, p is their momentum, m is their mass value, while c is the speed of light. $^3_\Lambda$H and $^3_\Lambda\overline{\mathrm{H}}$ samples are combined together to get a better statistics with the assumption of the same lifetime of $^3_\Lambda$H and $^3_\Lambda\overline{\mathrm{H}}$ based on the CPT symmetry theory. The measured yield is corrected with the tracking efficiency and acceptance of TPC, as well as the reconstruction efficiency of $^3_\Lambda$H and $^3_\Lambda\overline{\mathrm{H}}$. Then, the $l/(\beta\gamma)$ distribution can be fitted with an exponential function to extract the lifetime parameter $c\tau$. The best fitting with χ^2 minimization method results in $c\tau = 5.5^{+2.7}_{-1.4} \pm 0.08$, which corresponds to a lifetime of $182^{+89}_{-45} \pm 27$ ps as shown in Fig. 6. Figure 6 shows a comparison between the present measurement and theoretical calculation [27, 28], as well as the previous measurements [29–34]. It seems that the present measurement of $^3_\Lambda$H lifetime is consistent with the calculation with phenomenological $^3_\Lambda$H wave function [27] and a more recent three-body calculation [28]. The result is also comparable with the lifetime of free Λ within errors.

High production rate of $^3_\Lambda$H ($^3_\Lambda\overline{\mathrm{H}}$) due to equilibration among strange quarks and light quarks (u,d) is proposed to be a signature of the formation of QGP [18, 35]. The baryon strangeness correlation factor can be extracted by comparing the yields of $^3_\Lambda$H and ^{3}He. On the other hand, a recent calculation [36] indicates that the strangeness population factor, $S_3 = {}^3_\Lambda\mathrm{H}/({}^3\mathrm{He} \times \Lambda/p)$, is an effective tool to distinguish QGP phase and pure hadronic phase. Figure 7 depicts the excitation function of particle ratios for the STAR data and other previous measurements [37–39]. The value of S_3 is near unity at RHIC energy, while the same factor is only 1/3 at AGS energy, indicating that the phase space population of strangeness are comparable with light quarks at RHIC.

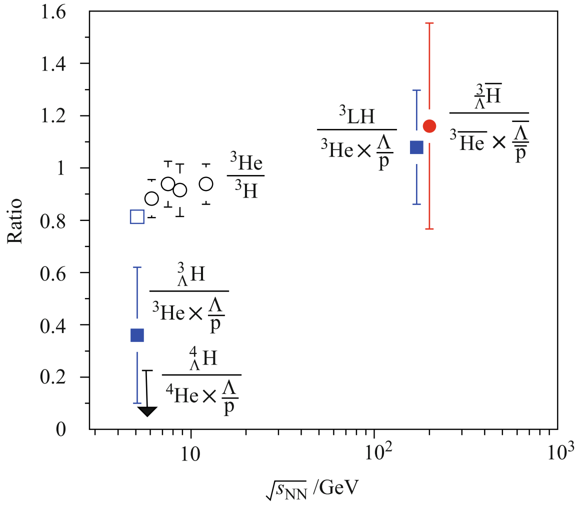

Fig. 7 Particle ratios versus center of mass energy per nucleon-nucleon collision. The data points besides this measurement are taken from Refs. [37–39]. Only statistical error are presented in the plot. Taken from Ref. [18], Copyright © 2010 American Association for the Advancement of Science.

5 Observation of $^4\overline{\mathrm{He}}$

The STAR collaboration also reported its observation of

$^4\overline{\text{He}}$ nucleus [19, 21] in April 2011, with 10 billion gold-gold collisions taken in the year 2007 and 2010. In addition to the particle identification method by combining energy loss ($\langle \mathrm{d}E/\mathrm{d}x \rangle$) and rigidity provided by TPC, the observation of $^4\overline{\text{He}}$ nucleus relies on the measured traveling time of tracks given by the barrel TOF [40], which is composed of 120 trays, surrounding the TPC. With the barrel TOF, the mass value of particles can be calculated via $m^2 = p^2(t^2/L^2 - 1)$ (where t and L are the time of flight and path length of tracks, respectively) for particle identification. On the other hand, the online high level trigger (HLT) was employed to perform preferential selection of collisions, which contains tracks with charge $Ze = \pm 2e$ for fast analysis. The trigger efficiency for $^4\overline{\text{He}}$ is about 70% with respect to offline reconstruction, with selection rate less than 0.4%. Figure 8 presents the $\langle \mathrm{d}E/\mathrm{d}x \rangle$ versus rigidity ($p/|Z|$) distribution. The colored bands stand for the helium sample collected by HLT. A cut of the DCA less than 3 cm for negative tracks (0.5 cm for positive tracks) is used to reject the background. In the left panel, 4 $^4\overline{\text{He}}$ candidates are identified and well separated from $^3\overline{\text{He}}$ at the low momentum region. While a clear ^{4}He signal is presented and centered around the expected $\langle \mathrm{d}E/\mathrm{d}x \rangle$ value of ^{4}He in the right panel.

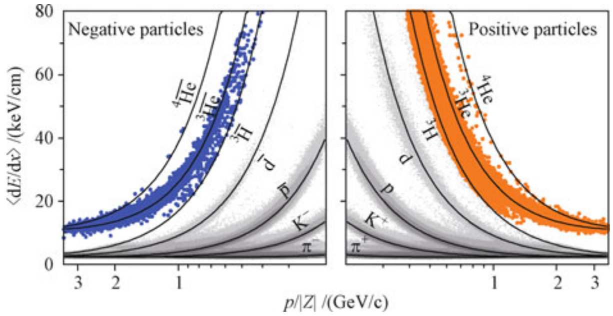

Fig. 8 $\langle \mathrm{d}E/\mathrm{d}x \rangle$ as a function of $p/|Z|$ for negatively charged particles (left panel) and positively charged particles (right panel). The black curves represent the expected values for each particle species. The lower edges of the colored bands correspond to the HLT's online calculation of 3σ below the $\langle \mathrm{d}E/\mathrm{d}x \rangle$ band center for ^{3}He. The grey bands indicate the $\langle \mathrm{d}E/\mathrm{d}x \rangle$ of deuteron, proton, kaon, pion from Minimum bias events at 200 GeV. Reproduced from Ref. [19], Copyright © 2011 Nature Group.

The $\langle \mathrm{d}E/\mathrm{d}x \rangle$ of ^{3}He ($^3\overline{\text{He}}$) and ^{4}He ($^4\overline{\text{He}}$) merge together at higher momentum region, and $n_{\sigma_{\mathrm{d}E/\mathrm{d}x}}$, which is defined as $n_{\sigma_{\mathrm{d}E/\mathrm{d}x}} = \frac{1}{R}\ln(\langle \mathrm{d}E/\mathrm{d}x \rangle / \langle \mathrm{d}E/\mathrm{d}x \rangle^B)$ (R is the resolution of $\langle \mathrm{d}E/\mathrm{d}x \rangle$) is used for further particle identification. Figure 9 shows the combined particle identification with $n_{\sigma_{\mathrm{d}E/\mathrm{d}x}}$ and $mass^2/Z^2$ value distribution. Two clusters of $^4\overline{\text{He}}$ and ^{4}He located at $n_{\sigma_{\mathrm{d}E/\mathrm{d}x}} = 0$, $mass^2/Z^2 = 3.48$ (GeV/c^2)^2 can be clearly separated from $^3\overline{\text{He}}$ and ^{3}He as well as ^{3}H and $^3\overline{\text{H}}$, which are presented in the top panel and bottom panel. By counting $^4\overline{\text{He}}$ signal with the cuts window $-2 < n_{\sigma_{\mathrm{d}E/\mathrm{d}x}} < 3$ and 2.82 (GeV/c^2)^2 $< mass^2/Z^2 <$ 4.08 (GeV/c^2)^2 as indicated in the top panel, 16 $^4\overline{\text{He}}$ candidates are identified. Together with 2 $^4\overline{\text{He}}$ candidates detected by TPC alone in the year 2007, which is presented in the figure, 18 $^4\overline{\text{He}}$ candidates are observed by the STAR experiment. So far, $^4\overline{\text{He}}$ is the heaviest antimatter nucleus observed in the world. Right after the public report of $^4\overline{\text{He}}$ from the STAR collaboration, the LHC-ALICE collaboration also claimed the observation of 4 $^4\overline{\text{He}}$ particles [41].

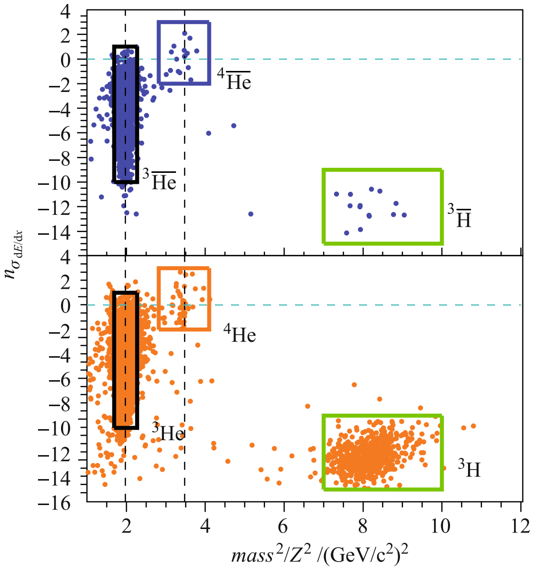

Fig. 9 Top (bottom) panel shows the $n_{\sigma_{\mathrm{d}E/\mathrm{d}x}}$ versus $mass^2/Z^2$ distribution for negative (positive) particles. The horizontal dashed lines mark the $n_{\sigma_{\mathrm{d}E/\mathrm{d}x}} = 0$, while the vertical ones stand for the theoretical mass values of ^{3}He($^3\overline{\text{He}}$) and ^{4}He($^4\overline{\text{He}}$). The signals of $^4\overline{\text{He}}$ and ^{4}He are counted in the cuts window of $-2 < n_{\sigma_{\mathrm{d}E/\mathrm{d}x}} < 3$. and $2.82(\mathrm{GeV/c^2})^2 < mass^2/Z^2 < 4.08(\mathrm{GeV/c^2})^2$.

6 Effort to search for antinuclei in Cosmic rays

As we discussed in the above sections, most efforts on hunting antinuclei were realized in high-energy nuclear physics laboratories. Nevertheless, it is still a dream to capture any antinucleus in cosmos. The search of $^4\overline{\text{He}}$ and heavier antinucleus in universe is one of the major motivations of space shuttle based apparatus such as the Alpha Magnetic Spectrometer [6]. Both the RHIC-STAR experimental result and model calculation provide a background estimation of $^4\overline{\text{He}}$ for the future observation in Cosmos radiations [19]. Recently, the effort to search for the Cosmic-Ray Antideuterons and Antihelium by the Balloon-borne Experiment with Superconducting Spectrometer (BESS) collaboration has been made [42, 43]. However, neither Antideuterons candidate was found using data collected during four BESS balloon flights from 1997 to 2000 [42], nor Antihelium candidate was found in BESS-Polar I data among 8.4×10^6 $|Z| = 2$ nuclei from 1.0 to 20 GV (absolute rigidity) or in BESS-Polar II data among 4.0×10^7 $|Z|= 2$ nuclei from 1.0 to 14 GV [43]. They derived an upper limit of 1.9×10^{-4} (m^2·s·sr GeV/nucleon)$^{-1}$ for the differential flux of Cosmic-Ray Antideuterons, at the 95% confidence level, between 0.17 and 1.15 GeV/nucleon at the top of the atmosphere [42]. For antihelium, assuming antihelium to have the same spectral shape as helium, a 95% confidence upper limit to the possible abundance of antihelium relative to helium of 6.9×10^{-8} was determined combining all BESS data, including the two BESS-Polar flights. With no assumed antihelium spectrum and a weighted average of the lowest antihelium efficiencies for each flight, an upper limit of 1.0×10^{-7} from 1.6 to 14 GV was determined for the combined BESS-Polar data. Under both antihelium spectral assumptions, these are the lowest limits obtained to date [42]. Figure 10 shows the new upper limits of antihelium/helium from the BESS experiment [42]. It seems very difficult to hunt anti-helium in cosmos.

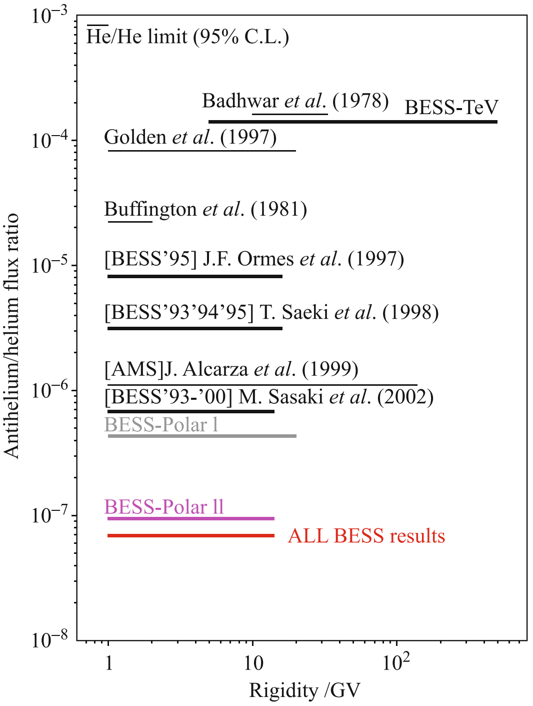

Fig. 10 The new upper limits of antihelium/helium at the TOA calculated assuming the same energy spectrum for He as for He with previous experimental results. The limit calculated with no spectral assumption is about 25% higher. Reproduced from Ref. [43], Copyright © 2012 American Physical Society.

7 Trap of antihydrogen atoms

Parallel to huge efforts of searching for the antimatter nuclei in the cosmos and laboratory, some scientists are thinking how to build the antimatter atom and make it trapped. Antihydrogen, the simplest form of antiatoms, which is the bound state of an antiproton and a positron, was reported to be produced by the LEAR in 1996 [44] and at low energies at CERN since 2002 [45, 46]. Antihydrogen is of interest for use in a precision test of nature's fundamental symmetries which is one of the most important projects of experiments in physics. In the standard model of particle physics, all properties of a particular physical process should be identical under the operation of charge conjugation, parity reflection, and time reversal (CPT). In nuclear physics, all properties of hydrogen including the fine structure and hyperfine structure are known at a high precision. A precise comparison between antihydrogen and hydrogen spectrum is one of the best ways to measure the possible CPT violation. The first confinement of antihydrogen with a trap time of 172 ms was demonstrated by the ALPHA experiment in 2010 [47] based on the antiproton decelerator facility. The most recent results with a confine time of 1000s was presented by the same collaboration [48], which is a big step towards the measurement of the antihydrogen properties. On the other hand, the mutual repulsive force between antimatter and matter (anti-gravity) was proposed, and many theoretical work has been done [47, 49] since the first observation of antimatter. However, no experimental result can be obtained until now. The successful trap of antihydrogen atoms provides a method to measure the gravitational effects by reducing the antihydrogen temperatures to the sub mK level in the way of adiabatic cooling.

8 Production mechanisms of antimatter light nuclei

Antimatter particles including $\bar{e}$, $\bar{p}$, $\bar{d}$, $^3\overline{\text{He}}$, $^3_{\bar{\Lambda}}\bar{\text{H}}$, $^4\overline{\text{He}}$ and antihydrogen atoms were observed in the past eighty years based on different kinds of sources and detectors. Most of these antimatter particles were produced by nucleon–nucleon reactions, where their production rate can be described by both thermodynamic model and coalescence model. In thermodynamic model, the system created is characterized by the chemical freeze-out temperature (T_{ch}), kinetic freeze-out temperature (T_{kin}), as well as the baryon and strangeness chemical potential μ_B and μ_S, respectively. (Anti)nucleus is regarded as an object with energy $E_A = Am_p$ (A is the atomic mass number, m_p is the mass of proton) emitted by the fireball [50]. The production rate are proportional to the Boltzmann factor $\mathrm{e}^{-m_pA/T}$ as shown in Eq. (1),

$$E_A\frac{\mathrm{d}^3N_A}{\mathrm{d}^3P_A} = \frac{gV}{(2\pi)^3}E_A\mathrm{e}^{-m_pA/T} \tag{1}$$

where P_A and g are the momentum and degeneracy of (anti)nucleus, V is the volume of the fireball. In coalescence picture, (anti)nucleus is formed by coalescence at the last stage of the system evolution since there exists strong correlation between the constituent nucleons in their phase space [15, 51, 52]. The production probability is described by Eq. (2),

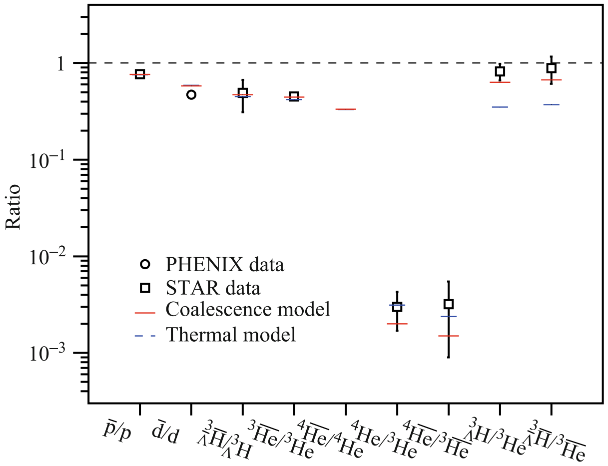

Fig. 11 The comparison of particle ratios between data and model calculations. The data points are taken from the STAR and the PHENIX experiments [18, 19, 14, 53]. The coalescent results are based on naive coalescence algorithm with a momentum difference lower than 100 MeV and a coordinator space difference less than $2R$ (R is the nuclear force radius), while the thermal predication is taken from Ref. [50]. Reproduced from Ref. [55], Copyright © 2012 American Physical Society.

$$E_A\frac{\mathrm{d}^3N_A}{\mathrm{d}^3P_A}=B_A\left(E_p\frac{\mathrm{d}^3N_p}{\mathrm{d}^3P_p}\right)^Z\left(E_n\frac{\mathrm{d}^3N_n}{\mathrm{d}^3P_n}\right)^{A-Z} \tag{2}$$

where $E\frac{\mathrm{d}^3N}{\mathrm{d}^3p}$ stands for the invariant yield of nucleons or (anti)nucleus, Z is the atomic number. And, p_A, p_p, and p_n are the momentum of (anti)nucleus, protons and neutrons, with the assumption of $p_A = A\times p_p$. B_A is the coalescence parameter.

Relative particle production abundance of (anti) nucleus are explored based on thermal model and coalescence model, and compared with data taken at RHIC. Figure 11 shows the particle ratios of (anti)nucleus. Both thermal model and coalescence model can fit the antinucleus to nucleus ratios at RHIC energy. While the coalescence model has a better description for ${}^3_{\Lambda}\mathrm{H}/{}^3\mathrm{He}$ and ${}^3_{\bar\Lambda}\overline{\mathrm{H}}/{}^3\overline{\mathrm{He}}$ than the thermal model [55]. In a microscopic picture, both coalescent and thermal production of (anti)nucleus predict an exponential trend for the production rate as a function of baryon number. The exponential behavior of (anti)nucleus production rate in nuclear nuclear reaction has been manifested in Fig. 12, which depicts the invariant yields ($\mathrm{d}^2N/(2\pi p_T\mathrm{d}p_T\mathrm{d}y)$) evaluated at the average transverse momentum ($p_T/|B| = 0.875$ GeV/c) region versus baryon number distribution. The solid symbols represent results reproduced by the coalescence model, which fits the data points very well. By fitting the model calculation with an exponential function $\mathrm{e}^{-r|B|}$, a reduction rate of 1692 (1285) can be obtained for each additional antinucleon (nucleon) added to antinucleus (nucleus), compared to $1.6^{+1.0}_{-0.6}\times10^3$ ($1.1^{+0.3}_{-0.2}\times10^3$) for nucleus (and antinucleus) obtained by the STAR experiment. The yield of next stable antinucleus (antilithium-6) is predicted to be reduced by a factor of 2.6×10^6 compared to ${}^4\overline{\mathrm{He}}$, and is impossible to be produced within current accelerator technology. The excitation of (anti)nucleus from a highly correlated vacuum was discussed in reference [54]. This new production mechanism can be tested with the measurement of the production rate of (anti)nucleus. Any deviation of the production rate of (anti)nucleus from usual reduction rate may indicate the existence of the direct excitation mechanism. On the other hand, the low production rate of ${}^4\overline{\mathrm{He}}$ antinucleus created by nuclear interaction indicate that any observation of ${}^4\overline{\mathrm{He}}$ or even heavier antinucleus should be a great hint of the existence of large amount of antimatter somewhere in the Universe.

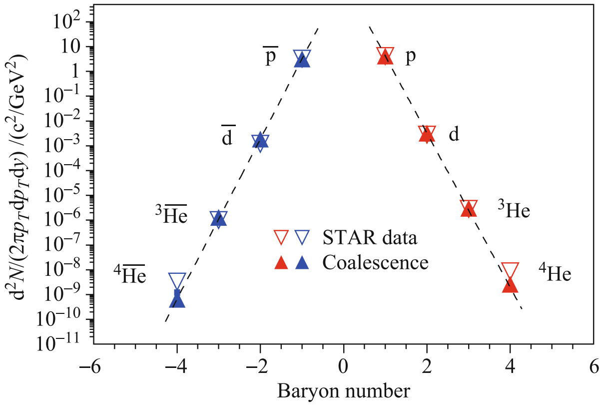

Fig. 12 Invariant yields $\mathrm{d}^2N/(2\pi p_T\mathrm{d}p_T\mathrm{d}y)$ of (anti)nucleus at the average transverse momentum region ($p_T/|B| = 0.875\mathrm{GeV/c}$) as a function of baryon number (B). The open symbols represents the data points extracted by the STAR experiment at RHIC energy, while solid ones are reproduced by coalescence model. The lines represent the exponential fit for our coalescence results of positive particles (right) and negative particles (left) with formula $\mathrm{e}^{-r|B|}$. Reproduced from Ref. [55], Copyright © 2012 American Physical Society.

9 Conclusions and perspectives

We briefly review the discovery history of antimatter, including positron that is the first antimatter observed [4, 5], antihelium-4 that is the heaviest antimatter nucleus observed so far [19], as well as anti-hypertriton that is the first antimatter hypernucleus [18]. With the increase of mass of antimatter particles, the difficulty of observation becomes much larger. With the increase of accelerator technology and beam energy, the detection of heavier antimatter nuclei becomes feasible. Antihypertriton and antihelium-4 are two good examples for antimatter detection with the present relativistic heavy ion collision facility. In the viewpoint of antimatter production, thermal model and coalescence model can basically describe the production yield of antimatter and antimatter-matter ratio. In our recent calculation based on the hydrodynamic motivated BlastWave model coupled with a coalescence model at RHIC energy, we demonstrate that the current approach can reproduce the differential invariant yields and relative production abundances of light antinuclei and antihypernuclei [55]. The exponential behavior of the differential invariant yields versus baryon number distribution is studied. By extrapolating the distribution to $B = -6$ region, the production rate of $^6\overline{\mathrm{Li}}$ in high energy heavy ion collisions is about 10^{-16}, and seems impracticable to be observed within current accelerator technology. As addressed in Section 5, the observation of $^4\overline{\mathrm{He}}$ and even heavier antinuclei in Cosmic rays is a great hint of the existence of massive antimatter in Universe. The model calculations and experimental measurements in high energy heavy ion collisions can simulate the interactions between high energy protons and interstellar materials. Thus our results provide a good background estimation for the future observation of $^4\overline{\mathrm{He}}$ and even heavier antinuclei in Universe.

Acknowledgements This work was partially supported by the National Natural Science Foundation of China (Grant Nos. 11035009, 11220101005, 10875160, 10805067, 10975174, 11275250, and 10905085), the Knowledge Innovation Project of Chinese Academy of Sciences under Grant No. KJCX2-EW-N01, and Dr. J. H. Chen was partially supported by the Shanghai Rising Star Project under Grant No. 11QA1408000.

References

1. A. Schuster, Nature, 1898, 58(1503): 367
2. P. A. M. Dirac, Proc. R. Soc. Lond., 1928, 117(778): 610
3. C. Y. Chao, Proc. Natl. Acad. Sci. USA, 1930, 16(6): 431
4. C. Y. Chao, Phys. Rev., 1930, 36(10): 1519
5. C. D. Anderson, Phys. Rev., 1933, 43(6): 491
6. S. Ahlen, V. M. Balebanov, R. Battiston, U. Becker, et al., Nucl. Instrum. Meth. Phys. Res. A, 1994, 350(1–2): 351
7. S. Orito, T. Maeno, H. Matsunaga, K. Abe, et al., Phys. Rev. Lett., 2000, 84(6): 1078
8. M. Casolino, P. Picozza, F. Altamura, A. Basili, et al., Adv. Space Res., 2008, 42(3): 455
9. D. E. Dorfan, J. Eades, L. M. Lederman, W. Lee, and C. C. Ting, Phys. Rev. Lett., 1965, 14(24): 1003
10. Y. M. Antipov, et al., Yad. Fiz., 1970, 12: 311
11. M. Antipov, S. P. Denisov, S. V. Donskov, Y. P. Gorin, et al., Nucl. Phys., 1971, B31(2): 235
12. B. Cork, G. R. Lambertson, O. Piccioni, and W. A. Wenzel, Phys. Rev., 1956, 104(4): 1193
13. N. K. Vishnevsky, et al., Yad. Fiz., 1974, 20: 694
14. J. Adams, et al. [PHENIX Collaboration], Phys. Rev. Lett., 2005, 94: 122302
15. B. I. Abelev, et al. [STAR Collaboration], arXiv:0909.0566 [nucl-ex]
16. O. Chamberlain, E. Segrè, C. Wiegand, and T. Ypsilantis, Phys. Rev., 1955, 100(3): 947
17. C. J. Kevane, Science, 1961, 133(3452): 580
18. B. I. Abelev, M. M. Aggarwal, Z. Ahammed, A. V. Alakhverdyants, et al. [STAR Collaboration], Science, 2010, 328(5974): 58
19. B. I. Abelev, et al. [STAR Collaboration], Nature, 2011, 473: 353
20. J. H. Chen, Nucl. Phys. A., 2010, 835(1–4): 117
21. L. Xue, J. Phys. G, 2011, 38(12): 124072
22. Y. G. Ma, Proceeding of NN2012 Conference, J. Phys.: Conf. Ser., 2012
23. G. B. Andresen, M. D. Ashkezari, M. Baquero-Ruiz, W. Bertsche, et al. [ALPHA Collaboration], Nat. Phys., 2011, 7(7): 558
24. T. Massam, T. Muller, B. Righini, M. Schneegans, and A. Zichichi, Nuovo Cim., 1965, 39(1): 10
25. J. K. Ahn, S. Ajimura, H. Akikawa, B. Bassalleck, et al,, Phys. Rev. Lett., 2001, 87(13): 132504
26. M. Anderson, J. Berkovitz, W. Betts, R. Bossingham,et al., Nucl. Instrum. Methods Phys. Res. A, 2003, 499(2-3): 659
27. R. H. Dalitz and G. Rajasekharan, Phys. Lett., 1962, 1(2): 58
28. H. Kamada, J. Golak, K. Miyagawa, H. Witala, and W. Glockle, Phys. Rev. C, 1998, 57(4): 1595
29. R. J. Prem and P. H. Steinberg, Phys. Rev., 1964, 136(6B): B1803
30. G. Bohm, J. Klabuhn, U. Krecker, F. Wysotzki, G. Coremans, J. Sacton, P. Vilain, J. H. Wickens, G. Wilquet, D. O'Sullivan, D. Stanley, D. H. Davis, T. Pniewski, T. Sobczak, and J. E. Allen, Nucl. Phys. B, 1970, 16(1): 46
31. G. Keyes, M. Derrick, T. Fields, L. Hyman, J. Fetkovich, J. McKenzie, B. Riley, and I. Wang, Phys. Rev. Lett., 1968, 20(15): 819
32. R. E. Phillips and J. Schneps, Phys. Rev., 1969, 180(5): 1307
33. G. Keyes, M. Derrick, T. Fields, L. Hyman, J. Fetkovich, J. McKenzie, B. Riley, and I. Wang, Phys. Rev. D, 1970, 1(1): 66
34. G. Keyes, J. Sacton, J. H. Wickens, and M. M. Block, Nucl. Phys. B, 1973, 67(2): 269
35. V. Koch, A. Majumder, and J. Randrup, Phys. Rev. Lett., 2005, 95(18): 182301
36. S. Zhang, J. H. Chen, H. Crawford, D. Keane, Y. G. Ma, and Z. B. Xu, Phys. Lett. B, 2010, 684(4–5): 224
37. T. A. Armstrong, K. Barish, S. Batsouli, S. Bennett, et al., Phys. Rev. C, 2004, 70(2): 024902
38. T. A. Armstrong, K. Barish, S. Batsouli, S. Bennett, et al., Phys. Rev. C, 2000, 61(6): 064908
39. V. I. Kolesnikov, J. Phys.: Conf. Ser., 2008, 110(3): 032010
40. B. Bonner, H. Chen, G. Eppley, F. Geurts, J. Lamas-Valverde, C. Li, W. J. Llope, T. Nussbaum, E. Platner, and J. Roberts, Nucl. Instrum. Meth. Phys. Res. A, 2003, 508(1–2): 181
41. N. Sharma, J. Phys. G, 2011, 38(12): 124189
42. H. Fuke, T. Maeno, K. Abe, S. Haino, et al., Phys. Rev. Lett., 2005, 95(8): 081101
43. K. Abe, H. Fuke, S. Haino, T. Hams, et al., Phys. Rev. Lett., 2012, 108(13): 131301

44. G. Baur, G. Boero, A. Brauksiepe, A. Buzzo, et al., Phys. Lett. B, 1996, 368(3): 251

45. M. Amoretti, C. Amsler, G. Bonomi, A. Bouchta, et al., Nature, 2002, 419(6906): 456

46. G. Gabrielse, N. S. Bowden, P. Oxley, A. Speck, C. H. Storry, J. N. Tan, M. Wessels, D. Grzonka, W. Oelert, G. Schepers, T. Sefzick, J. Walz, H. Pittner, T. W. Hänsch, and E. A. Hessels, Phys. Rev. Lett., 2002, 89(21): 213401

47. G. B. Andresen, M. D. Ashkezari, M. Baquero-Ruiz, W. Bertsche, et al., Nature, 2010, 468(7324): 673

48. G. B. Andresen, M. D. Ashkezari, M. Baquero-Ruiz, W. Bertsche, et al., Nat. Phys., 2011, 7(7): 558

49. M. Villata, et al., Europhys. Lett., 2001, 94: 2011

50. A. Andronic, P. Braun-Munzinger, J. Stachel, and H. Stöcker, Phys. Lett. B, 2011, 697(3): 203

51. H. Sato, K. Yazaki, et al., Phys. Lett. B, 1981, 98(3): 153

52. R. Scheibl and U. Heinz, Phys. Rev. C, 1999, 59(3): 1585

53. J. Adams, M. M. Aggarwal, Z. Ahammed, J. Amonett, et al. [STAR Collaboration], Nucl. Phys. A., 2005, 757(1-2): 102

54. W. Greiner, Int. J. Mod. Phys. E, 1996, 5(01): 1

55. L. Xue, Y. G. Ma, J. H. Chen, and S. Zhang, Phys. Rev. C, 2012, 85(6): 064912